# Analysis and design of a drain water heat recovery storage unit based on PCM plates

S. Morales-Ruiz [b], J. Rigola [a], C. Oliet [a], A. Oliva [a,*],

[a] *Heat and Mass Transfer Technological Center (CTTC); Universitat Politècnica de Catalunya - BarcelonaTech (UPC) ETSEIAT, Colom 11, 08222 Terrassa, Barcelona, Spain*

[b] *Termo Fluids S.L., Avda. Jacquard 97 1-E, 08222 Terrassa, Barcelona, Spain*

**Abstract**

This paper is focused on the detailed analysis of a PCM plate heat storage unit with a particular configuration, looking for the maximum contact area with the fluid (water) and the minimum volume to be used in a real household application. In that sense, a numerical study of the thermal and fluid dynamic behaviour of the water flow and the PCM melting-solidification processes, together with the thermal behaviour of the solid elements of the unit, has been carried out. On the other hand, an experimental set-up has been designed and built to validate the numerical model and characterize the performance of the heat storage unit. The purpose of the numerical and experimental study is to present a serie of results to describe the heat storage unit performance in function of the time. Thus, after a preliminary design study three different cases have been simulated and tested. A 7.2% of discrepancy between numerical

* Corresponding author. Tel: +34 93 7398192; fax: +34 93 739 89 20
*Email address:* cttc@cttc.upc.edu (A. Oliva).

results and experimental data has been evaluated for the heat transfer. The PCM heat storage unit designed is capable to store approx. 75% of the thermal energy from the previous process wasted water heat, and recover part of it to supply around 50% of the thermal energy required to heat up the next process.

*Key words:* Heat storage unit, Phase change material (PCM), Thermal performance analysis, Drain water heat recovery (DWHR), Numerical simulation, Experimental set-up.

---

## 1 Introduction

The high cost of the energy, the excessive use of natural resources, the dispatchability of renewable energies and the corresponding demand of wasted heat recovery systems have encouraged the development of new thermal storage technology. The phase change material (PCM) heat storage system takes advantage of both sensible and latent heat to store thermal energy increasing efficiency and reducing space.

Latent heat thermal energy storage is an attractive technique because it has a high energy storage density, which can be between 5 and 14 times higher than a conventional sensible heat storage material [1]. However, the use of PCMs has an important drawback, which is the low thermal conductivity which means low energy charging and discharging rate. Other important disadvantages of the PCMs are: density changes, poor stability under extended cycling, phase segregation and cost, amongst others.

The study of PCMs began seven decades ago but did not receive much attention until the energy crisis of late 1970s and early 1980s [2], when different experimental and numerical studies on melting and solidification processes of

some PCMs were published [3, 4]. Currently, there are different type of applications where the PCMs are used, i.e. solar heating systems, cooling and heating (using off-peak rate), thermal protection of food, thermal protection of electronic devices, cooling of engines, thermal comfort in vehicles, and medical applications between others [5–8].

Different types of heat storage systems based on PCMs are described in the technical literature, where physical characteristics, thermal performance and evaluating methodology have been shown. A compilation of typical configurations of PCM heat storage systems are presented in [9–14], covering geometries e.g.: flat-plate, shell-and-tube, shell-and-rod, and shell-and-spheres. The numerical analysis of a PCM encapsulated in different forms has been carried out by means of different numerical methods: the fixed grid and time step method [12], the efficient heat capacity [13], one-dimensional and bi-dimensional conduction analysis [15, 16], and the enthalpy method [10, 13, 17–21]. Different experimental studies to validate the proposed numerical models and to evaluate the thermal performance of heat storage units have been carried out [10,12,13,15,20–22]. The influence and advantages of applying multi-PCMs in comparison with a single PCM in two different configurations of heat storage units (shell-and-tube and zigzag plate) used in an air-cooling application have been presented [18, 20].

Around 20-26% of the total energy consumption in a typical home is consequence of water heating activities [23]. For that reason, there are many studies in which different technologies have been tested in order to save energy used to heat domestic water. Some of these technologies are: solar water heating (SWH), gas boilers, heat pumps, immersion heater, exhausted heat recovery systems and drain water heat recovery (DWHR) systems [14, 16, 19, 23–28].

The DWHR system is an attractive household technology, which can help to reduce the energy consume and environmental impact. The conventional DWHR

units are based on a heat exchanger, which use cold water coils wrapped around a hot water drain [23, 29–31], some of these units use a hot water tank (HWT) as a storage device. A DWHR system recovers heat from a waste water volume, which can be reused in water preheating, obtaining efficiency between 17-75% in function of several factors [23]. A high variation of the DWHR efficiency has been reported by investigators, in which the DWHR efficiency depends on the kind of device, orientation, and specific characteristics of the waste water (flow rate and temperature) [23, 29–33]. The lowest efficiency value is obtained with horizontal DWHR, whilst the highest value is achieved with vertical DWHR. There are different sources of waste water in household applications, i.e.: bath/shower, sink, washing machine or dish-washing machine [23, 32, 33].

Although the authors have not found specific information about DWHR systems based on PCMs and their use in real application into the household technology as a medium to save energy, looking for in the technical literature, the use of PCMs as an auxiliary device to storage energy in a solar domestic hot water (SDHW) system has been reported [14, 19]. These works have analysed the thermal behaviour of this kind of unit and exposed the main advantages of using PCM in solar domestic hot water systems.

The main advantage of applying PCM in any kind of heat storage system is the capacity to accumulate thermal energy with high energy density in a well defined temperature range, due to the fact of taking advantage of both sensible and latent heat. This important feature is reflected in improved thermal performance and the volume reduction of the unit [14, 19].

This paper is focused on a detailed analysis of a PCM plate heat storage unit with a particular configuration, looking for the maximum contact area with the water flow and the minimum volume. The design proposed is based on a group of PCM plate capsules, which are arranged making up a thermal system.

The heat exchanger process occurs between the PCM plate capsules and the water flow. The heat storage unit is designed to work with a specific mass of drain/grey water as a heat source (wasted heat). An interesting design is achieved using a numerical and experimental strategy to develop a particular storage and recovery unit, which is based on PCM plates. The PCM plates are organized in a specific arrangement to generate a series of channels between two PCM plates by means of metallic supports. The PCM plate heat storage unit designed can be used as a DWHR system coupled to a real household application. The thermal performance of this unit is evaluated, achieving a heat recovery ratio similar to highest values reported in technical literature by researchers in the field of DWHR systems.

The numerical model is based on: i) a one-dimensional and transient integration of the conservative equations (mass, momentum and energy) for the water flow inside of the channels [34–36]; ii) two-dimensional and transient integration of the conservative equations (mass, momentum and energy) for the PCM using the Stephan condition at the interface [37–40]; iii) two-dimensional and transient integration of the energy conservation equation for the solid elements. A group of empirical correlations obtained from technical literature [41–43] has been used to evaluate the heat transfer coefficient and the friction factor. A preliminary design study was carried out with the aim of defining a suitable PCM, an optimum PCM plates and the prototype unit geometry. Numerical results of the whole storage unit are shown, where the temperature of the fluid flow and the temperature and melting fraction distribution of the PCM plate capsules are presented.

An experimental facility has been designed to measure the variables that characterize the working conditions of the PCM heat storage unit. A description of the experimental unit is presented, together with detailed information about instrumentation used. The experimental data obtained is used to identify the

thermal performance of the heat storage unit designed, as well as to validate the mathematical model proposed in this paper.

## 2 Mathematical Formulation

This section presents the mathematical formulation for the whole heat storage unit, i.e. the fluid flow, the plates and the PCM. A final subsection shows the empirical inputs needed to take into account fluid flow and solid interactions.

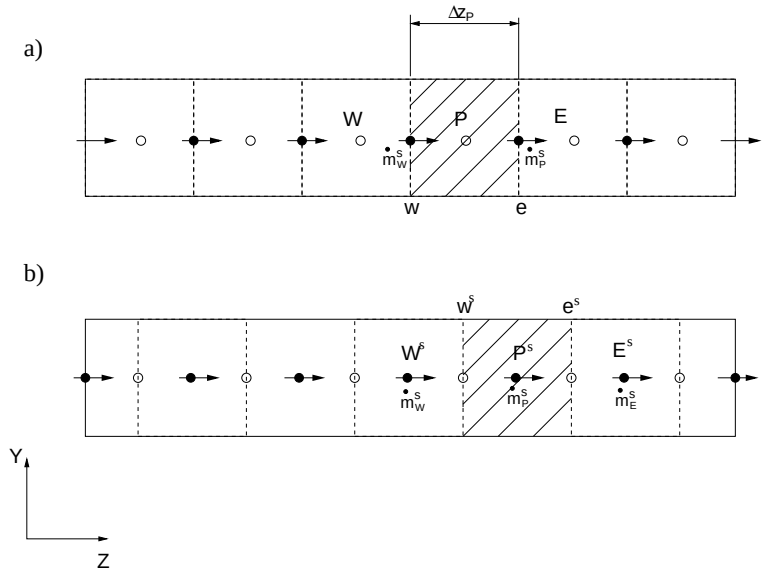


Fig. 1. Schematic representation of the meshes used in the discretization of the fluid flow: a) Main control volumes for pressure and energy, b) Staggered control volumes for mass flux. Symbol (○) indicates the node of the main mesh, and (●) indicates the node of the staggered mesh.

The mathematical formulation for the fluid is based on the conservation equations of mass, linear momentum and energy, where the main assumed hypothesis are: one-dimensional flow, negligible axial heat conduction and viscous dissipation, negligible pressure drop generated by the elbows and negligible heat radiation. These equations are integrated on the basis of staggered meshes as required by SIMPLEC methodology [44] to avoid checker-board solutions. In

this way, the domain is split into a number of control volumes (CVs). Mass and energy equations are discretized over the main CVs as shown in Fig. 1a, while momentum equation is discretized over the staggered CVs as shown in Fig. 1b.

The mathematical formulation for the PCM is based on the conservation equations of mass, linear momentum and energy. The thermal behaviour of the PCM is solved on a fix grid using an enthalpy method. The energy equation is expressed in function of the PCM enthalpy. The main assumed hypothesis are: Newtonian fluid, two-dimensional and transient flow, laminar flow, negligible viscous dissipation, and the Boussinesq approximation. These equations are discretized over the CVs indicated in Fig. 2.

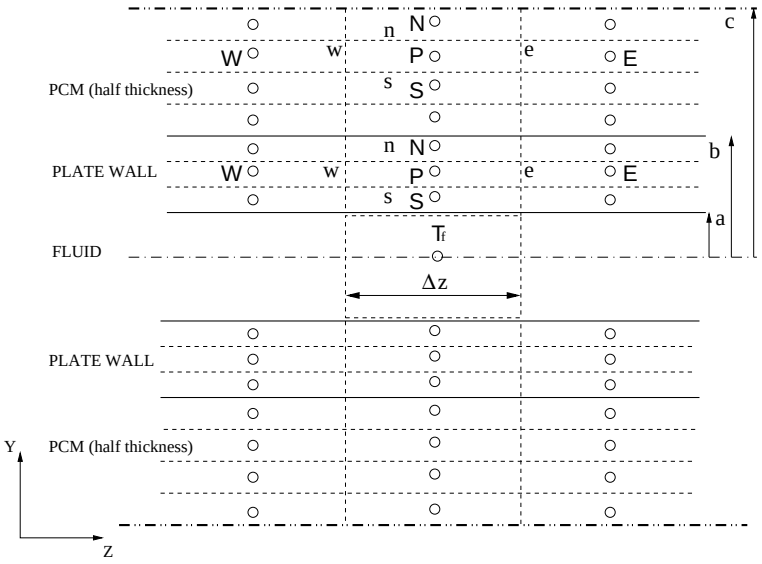


Fig. 2. Discretization of the solid elements, PCM and fluids. Main nodes assigned to the selected CVs are denoted by P, while W,E,N,S indicated their neighbours. Cell-faces are denoted by lower-case letters (w,e,n,s).

The mathematical formulation for the plate is based on the heat conduction equation, where the main assumed hypothesis are: two-dimensional temperature distribution and negligible heat radiation between plates and the exterior. This equation is discretized over the CVs indicated in Fig. 2.

A strategy has been used to simplify the simulation of the whole PCM plate heat storage unit. It corresponds to the development in a single channel of length $L$ ($L = N_p \cdot L_p$) the series of channels configured between $N_p$ PCM plate capsules (each one of length $L_p$). This single channel is configured between two PCM plates considering a half of the real PCM plate capsule thickness (adiabatic condition is assumed in the central section). This simplification neglected the flow direction changes into the PCM plate heat storage unit and the particularities of the first and last water channels (PCM on one side, heat losses to environment on the other side).

### *2.1 Fluid flow*

The semi-discretized and temporal form of the mass, momentum and energy conservations equations of the fluid flow inside the channels are presented:

$$V\frac{\partial \tilde{\rho}_P}{\partial t} + \dot{m}_e - \dot{m}_w = 0 \tag{1}$$

$$V\frac{\partial \tilde{\rho}\tilde{v}}{\partial t} + \dot{m}^s_e v^s_e - \dot{m}^s_w v^s_w = (p_P - p_E)A - \bar{\tau}_P 2H\Delta z - mg\sin\theta \tag{2}$$

$$V\frac{\partial \tilde{\rho}_P \tilde{e}_P}{\partial t} + \dot{m}_e e_e - \dot{m}_w e_w = \bar{\dot{q}}_P 2H\Delta z + V\frac{\partial \tilde{p}}{\partial t} \tag{3}$$

where $\tilde{e}_P$ represents the total specific energy ($e = h + e_c + e_{pot}$), $h$ is enthalpy, $e_c$ kinetic energy, $e_{pot}$ potential energy, $\tilde{\rho}_P$ is the density, $\bar{\dot{q}_P}$ is the heat flux transferred between fluid flow and plate, $p$ is the pressure, $\bar{\tau}_P$ is the shear stress, $\dot{m}_e$ and $\dot{m}_w$ are the mass flow at the east and west CV-faces respectively, $A$ is the cross sectional area, $H$ is the plate width, $V$ is the CV volume, and $\triangle z$ is the CV length. The mean values over the CV used in last equations are defined as:

$$\tilde{\rho}_P = \frac{1}{V}\int_{V_P} \rho dV \quad ; \quad \tilde{p}_P = \frac{1}{V}\int_{V_P} p dV$$
$$\tilde{e}_P = \frac{1}{\tilde{\rho}_P V}\int_{V_P} \rho e dV \quad ; \quad \bar{\dot{q}}_P = \frac{1}{\Delta z}\int_{z_w}^{z_e} \dot{q} dz \tag{4}$$

Transient terms are evaluated using a first order backward differencing scheme. Convective terms at the CV faces are evaluated using first or higher order schemes. The convective heat flux is integrated along the CV heat transfer surface using local heat transfer coefficients and nodal temperatures for the plate and the fluid. This methodology to solve the fluid flow has been used by the authors in other numerical studies [34–36], where the thermal and fluid dynamic behaviour of the single-phase flow and two-phase flow has been solved.

### *2.2 Plate*

To solve the plate temperature distribution, the energy equation is used. A differential form of the general heat conduction equation is expressed in function of temperature:

$$\rho c_p \frac{\partial T}{\partial t} = \frac{\partial}{\partial z}\left(\lambda \frac{\partial T}{\partial z}\right) + \frac{\partial}{\partial y}\left(\lambda \frac{\partial T}{\partial y}\right) \tag{5}$$

where the left hand side indicates the internal energy increase in the CV, while the right hand represents the heat flux through the CV-faces (west, east, north, and south). The edges of the plate are considered adiabatic. The interactions of the plate with PCM and fluid are also stated in the corresponding boundary conditions:

$$
\begin{aligned}
\left.\frac{\partial T}{\partial z}\right|_{(z=0,y,t)} &= \left.\frac{\partial T}{\partial z}\right|_{(z=L,y,t)} = 0 \\
-\lambda_{pl}\left.\frac{\partial T}{\partial y}\right|_{(z,y=a,t)} &= \alpha_f(T_f - T_P) \\
-\lambda_{pl}\left.\frac{\partial T}{\partial y}\right|_{(z,y=b,t)} &= -\lambda_{PCM}\left.\frac{\partial T}{\partial y}\right|_{(z,y=b,t)}
\end{aligned}
\tag{6}
$$

where $\alpha_f$ is the heat transfer coefficient, $T_f$ is the fluid temperature, $T_P$ is the plate temperature at node P, $L$ is the developed length, $\lambda$ is the thermal conductivity of the plate and PCM, and $b - a$ is the plate thickness (Fig. 2).

### *2.3 PCM*

The thermal behaviour of the phase change material is solved by means of the conservative mass, momentum and energy equations. The energy equation is expressed in function of the enthalpy [37–39], in which PCM enthalpy is taking into account the sensible and latent heat required for the phase change. Average and constant values of solid and liquid material properties are used (density and thermal conductivity) and a relation between PCM temperature and enthalpy is known. The expressions used are:

$$
\frac{\partial u}{\partial z} + \frac{\partial v}{\partial y} = 0 \tag{7}
$$

$$
\rho\frac{\partial u}{\partial t} + \rho u\frac{\partial u}{\partial z} + \rho v\frac{\partial u}{\partial y} = \frac{\partial p}{\partial z} + \mu\left(\frac{\partial^2 u}{\partial z^2} + \frac{\partial^2 u}{\partial y^2}\right) + B \cdot u \tag{8}
$$

$$
\rho\frac{\partial v}{\partial t} + \rho u\frac{\partial v}{\partial z} + \rho v\frac{\partial v}{\partial y} = \frac{\partial p}{\partial y} + \mu\left(\frac{\partial^2 v}{\partial z^2} + \frac{\partial^2 v}{\partial y^2}\right) + \rho g\beta(T - T_\infty) + B \cdot v \tag{9}
$$

$$\rho\frac{\partial h}{\partial t}+\rho u\frac{\partial h}{\partial z}+\rho v\frac{\partial h}{\partial y}=\lambda\left[\frac{\partial^2 T}{\partial z^2}+\frac{\partial^2 T}{\partial y^2}\right] \tag{10}$$

where $u$ and $v$ are the liquid velocities of the PCM, $p$ is the dynamic pressure, $B$ is a parameter which must be defined in a way that ensures a gradual slow down of velocities in the solidifying computational cells (B is zero in full liquid cells and B is a large value in full solid cells, thus forcing the velocities to be practically zero) [38, 40]. Assuming that the phase change solid-liquid or liquid-solid occurs between a small temperature range, the melting fraction can be defined as:

$$f_l=\begin{cases}1 & \text{for } T>T_{melt1}\\ 0 & \text{for } T<T_{melt2}\\ \frac{(h_p-h_{sol})}{(h_{liq}-h_{sol})} & \text{for } T_{melt2}<T<T_{melt1}\end{cases} \tag{11}$$

where $T_{melt1}$ is the PCM melting temperature, $T_{melt2}$ is the PCM solidification temperature, $h_p$ is the PCM enthalpy, and $h_{liq}$ and $h_{sol}$ are the liquid and solid enthalpy of the PCM, respectively.

The boundary conditions of the PCM are:

$$\begin{aligned} u_{(z=0,z=L,y=b,y=c,t)}&=v_{(z=0,z=L,y=b,y=c,t)}=0\\ \left.\frac{\partial h}{\partial z}\right|_{(z=0,y,t)}&=\left.\frac{\partial h}{\partial z}\right|_{(z=L,y,t)}=0\\ -\lambda_{pl}\left.\frac{\partial T}{\partial y}\right|_{(z,y=b,t)}&=-\lambda_{PCM}\left.\frac{\partial T}{\partial y}\right|_{(z,y=b,t)}\\ \left.\frac{\partial h}{\partial y}\right|_{(z,y=c,t)}&=0\end{aligned} \tag{12}$$

where $c-b$ is the PCM half thickness (Fig. 2).

*2.4 Empirical correlations*

The heat transfer coefficient ($\alpha_f$) used to calculate the heat flux transferred between the fluid flow and the plate and the friction factor used to calculate the shear stress ($\bar{\tau}_P$) between fluid and plate are evaluated from empirical information obtained from technical literature. The heat transfer coefficient has been obtained from [42], proposed to be used in small plate heat exchangers with intermating plates:

$$\alpha_f = \frac{Nu\lambda}{D_e} \text{ with: } \begin{cases} Nu_{lam} = 1.68(RePr\frac{D_e}{L_P})^{0.4}(\frac{\mu}{\mu_w})^{0.1} & \text{for } Re < 10 \\ Nu_{tur} = 0.2Re^{0.67}Pr^{0.4}(\frac{\mu}{\mu_w})^{0.1} & \text{for } Re > 100 \\ Nu = f(Re, Nu_{lam}, Nu_{tur}) & \text{otherwise} \end{cases} \quad (13)$$

where $Nu$ is the Nusselt number, $Re$ is the Reynolds number, $Pr$ is the Prandl number, $D_e$ is the hydraulic mean diameter, $L_p$ is the plate length, $\lambda$ is the thermal conductivity, $\mu$ is the bulk viscosity, and $\mu_w$ is the viscosity at plate temperature. Thus, the heat flux transferred between fluid flow and plate can be evaluated by means of the following expression $\bar{\dot{q}}_P = \alpha_f(T_f - T_P)$, where $T_f$ is the fluid temperature and $T_P$ is the plate temperature at the node centre.

The friction factor $f$ and shear stress $\bar{\tau}_P$ are evaluated from [42], proposed to be used in small plate heat exchangers with intermating plates:

$$\bar{\tau}_P = f\frac{\rho v^2}{2} \text{ with: } \begin{cases} f_{lam} = \frac{38}{Re} & \text{for } Re < 10 \\ f_{tur} = \frac{1.22}{Re^{0.252}} & \text{for } Re > 100 \\ f = f(Re, f_{lam}, f_{tur}) & \text{otherwise} \end{cases} \quad (14)$$

These empirical expressions have been chosen from literature due to the corrugate surface of the PCM plate capsules, similar to intermating plates geometry. In the transition regime the Nusselt number ($Nu$) and the factor friction ($f$) can be determined by interpolation between boundaries of the laminar and turbulent regimes.

## 3 Numerical Resolution Method

The global numerical algorithm to solve the whole system takes into account, in coupled manner, the thermal and fluid dynamic behaviour of the different elements. At the initial instant (t=0), pressure, mass flow rate, enthalpy or temperature of the fluid, plate temperature, and PCM melting fraction and temperature must be fully defined. The **fluid flow** is simulated by means of the numerical resolution of the equations (1) to (3) as a first step. The discretized equations are solved using the three diagonal matrix algorithm TDMA. The coupling between momentum and continuity is solved by means of the semi-implicit pressure-based method SIMPLEC [44]. The **plate** temperature is obtained from the numerical resolution of the equation (5). The discretized equation is solved by means of the SOR+TDMA solver.

The **PCM** is simulated by means of the numerical resolution of the equations (7 to 10) as a third step. These equations have been discretized and organized in a generic two-dimensional form. The set of algebraic equations is solved by means of the SOR+TDMA solver. The coupling between momentum and continuity is solved using a SIMPLEC method [44]. Next, the energy equation in function of enthalpy $h$ is solved. After that, an evaluation of the PCM temperature $T_{PCM}$ is carried out as a function of PCM enthalpy and the melting fraction $f_l$.

An iterative process should be made until the convergence criteria is reached

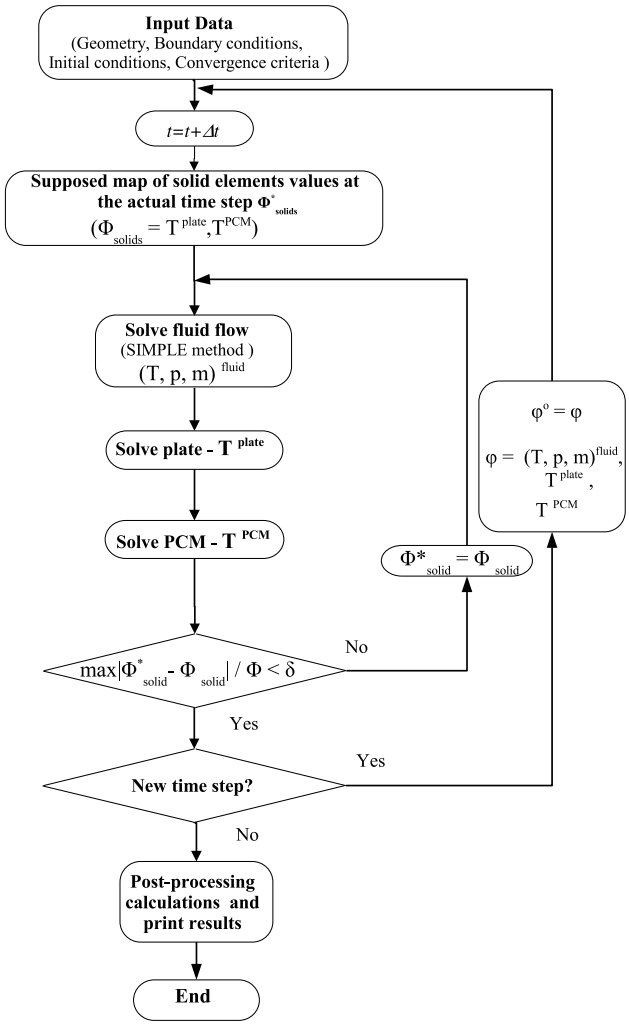


Fig. 3. Global numerical algorithm

in all elements. The convergence of the system is based on the maximum difference between the different local variables at the previous iteration $\phi^*$ and at the actual one $\phi$, i.e. $(max|\phi - \phi^*|/\phi) < \delta$, where a convergence criteria value ($\delta = 1e^{-6}$) has been used in all cases. The process runs step-by-step in the time direction until a steady-state or some specific period of time is reached. A representation of the numerical algorithm is depicted in Fig. 3.

## 4 Experimental Facility

The experimental facility was specifically oriented to study the thermal performance of the PCM plate heat storage unit proposed. The design of the test rig was performed considering the transient condition of the thermal process analysed, with the main aim of quantifying the thermal energy saved/released by the test unit during a period of time. The experimental data obtained is used also to validate the numerical modelling implemented to simulate the whole heat storage system. A detailed scheme of the experimental facility is shown in Fig. 4.

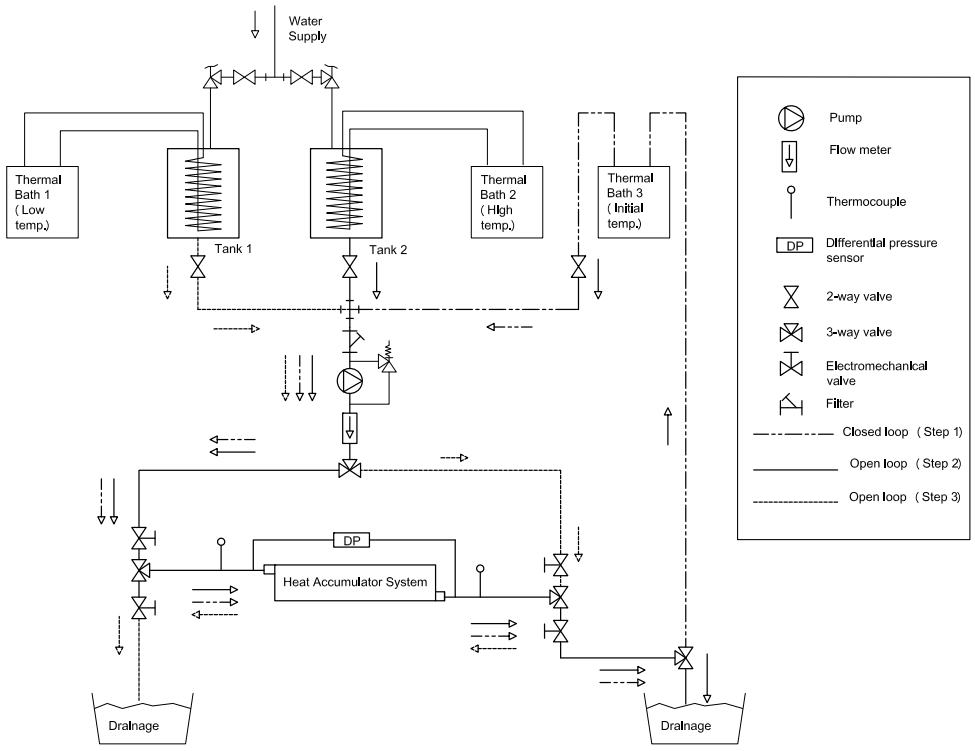


Fig. 4. Schematic representation of the experimental facility

The facility is formed by two 25 litres stainless steel tanks (a cold fluid tank and a hot fluid tank) which assure the supply of fluid to the heat storage system,

three different heat sources (thermal baths) working at different temperatures, a group of electromechanical valves to control the fluid flow sequence through the whole circuit, and a group of instruments to measure temperature, pressure and flow rate.

A copper helical coil has been located into each one of the tanks to heat/cool the fluid to the required temperature, by its connection to a thermal bath.

A group of four electromechanical valves have been used to control the water flow through the facility circuit. Depending on the condition (heat charge or discharge) part of the circuit is open supplying water at specific conditions (hot or cold) from tanks to the heat storage unit. Along the circuit different sensors of temperature, pressure and flow rate have been installed. Two thermocouples are located at the inlet and outlet of the heat storage unit to measure the water temperature. A Coriolis mass flow meter has been used for the water mass flow measurement. A differential pressure sensor has been used to evaluate the water pressure drop generated by the heat storage unit. Technical specifications of sensors and devices that make up the experimental facility are summarized in Table 1.

Table 1

Accuracy and devices specifications used in the experimental facility

| Device | Type | Range | Accuracy |
|---|---|---|---|
| Pump | Magnetic drive gear | up to 12 $lt/min$ | |
| Flow meter | Coriolis | up to 56 $kg/min$ | $\pm$ 0.041% F.S. |
| Thermocouples | K-Type | 10°C to 70°C | $\pm$ 0.3 °C |
| Differential pressure | Diaphragm | 0 to 248.0 $kPa$ | $\pm$ 0.04% F.S. |

An uncertainty analysis has been applied to evaluate the errors influence of the different variables measured on the experimental results, which is based

on a propagation error methodology proposed in the technical literature [45, 46]. The maximum uncertainty estimated for the heat transfer rate is around $\pm 5.98\%$ , whilst $\pm 4.73\%$ was obtained as a maximum uncertainty for the energy stored/recovered during the thermal charge or discharge processes.

### *4.1 Test procedure*

The heat storage unit has been tested following a procedure divided into three steps: i) *Initialization*, a water flow passes through the heat storage unit with the purpose of imposing an initial temperature in the test unit. The water flow used to impose this condition has been conditioned by thermal bath 3, see Fig. 4. After some minutes and verifying that the difference between the fluid flow temperature at the inlet and at the outlet of the heat storage unit is short enough, the experimental facility is ready to start the heat storage test; ii) *Thermal charge*, a prescribed water volume at high temperature flows from tank 2 to the heat storage unit. This fluid flow transfers part of its thermal energy to the heat storage unit (PCM plates). As a consequence, the fluid stream outlet temperature decreases; and iii) *Thermal discharge*, as soon as the hot water volume has passed through the circuit and the heat storage unit has been thermally charged, a second water volume at low temperature flows from tank 1 to the heat storage unit. This water stream flows in counter-current direction in comparison with the charge volume flow. When this cold fluid stream reaches the test unit, the PCM/plates transfer part of the thermal energy previously stored to the fluid stream in a thermal discharge process. As a consequence, the fluid stream outlet temperature increases.

There is a short transition period between each one of the three steps described above, when the water stream moves a water volume (2 litres approximately) at different thermal conditions than water prepared in the tanks. During this transition period the water volume is thrown directly to the drainage with-

out pass through the PCM Unit. Therefore, transition is not included in the numerical simulation as not affecting the storage unit.

## 5 Design of the PCM plate heat storage unit

The PCM plate heat storage unit designed is characterized by a parallelepiped-shaped outer casing configuration, inside which flows the fluid (water) in a single stream without branching. The heat storage unit consists of a metallic box manufactured with a stainless steel sheet. This device was designed to house a group of PCM plates in a specific arrangement to generate a series of channels between two PCM plates (Fig. 5). A number of metallic supports were welded to the metallic box to facilitate the accommodation and arrangement of the PCM plates into the box. These supports are arranged in parallel but pointing in opposite directions alternately, with the aim of leaving a gap between the PCM plates and the housing through which the fluid flows. The parallel arrangement and the opposite sense of the supports generates a circuit with rectangular section, which has a great ratio between the width and height of the section.

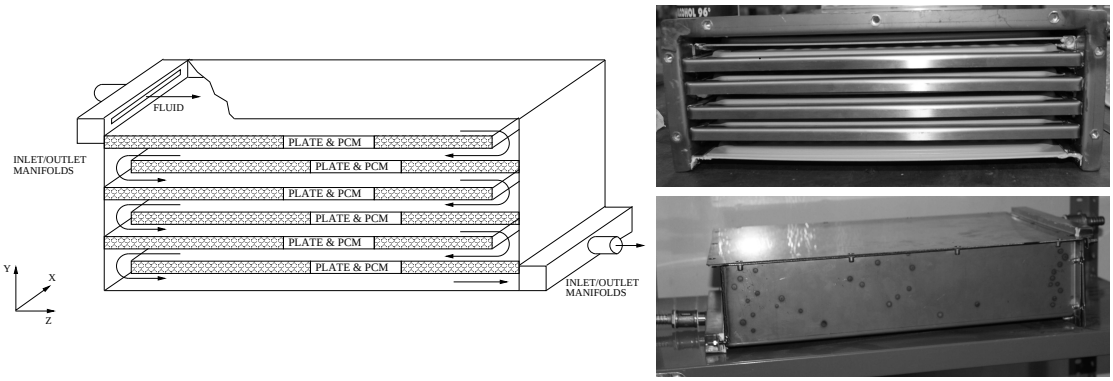


Fig. 5. PCM plate heat storage unit: schematic representation (left); and front and side views (right)

The PCM plate capsules consist of two slim aluminium sheets that make up a case to encapsulate a mass of phase change material. The distance between

PCM plate capsules is 5 mm, it ensures an equilibrated rate between heat transfer surface and PCM volume. The thickness of the PCM encapsulated should be taken into account in the design of the heat storage unit, because the low thermal conductivity of PCM affects unfavourably the phase change in rapid transient processes. If the phase change occurs only in the first few millimetres of thickness, much material will be wasted. Thermo-physical properties of the PCM encapsulated in an aluminium plate capsule are summarized in Table 2. These data were obtained from the technical data sheet of a commercial paraffin, which was supplied by the manufacturer.

Table 2

Thermo-physical properties of the PCM

| Material | Paraffin |
|---|---|
| Density liquid | 770 $kg/m^3$ |
| Density solid | 880 $kg/m^3$ |
| Specific heat liquid | 2400 $J/kgK$ |
| Specific heat solid | 1800 $J/kgK$ |
| Heat storage capacity | 174 $kJ/kg$ |
| Thermal conductivity | 0.2 $W/mK$ |
| Melting temperature range | 21°C to 24°C |

The fluid flow distribution in the heat storage unit has been analysed by visualization studies, where entry is determinated by a manifold (Fig. 6). The manifold chosen has a small slot to avoid non-regular distribution in the inner channel. The tested unit has been insulated appropriately to reduce the heat loss to the environment. The heat storage unit has been assembled with the experimental facility, which has been described in the previous section, with the aim of testing its thermal performance under specific working conditions.

Fig. 6. Manifold

### *5.1 Application specific design*

A preliminary numerical study was carried out with the aim of defining a suitable PCM plate heat storage unit design, which will be used as a thermal storage device in a domestic washing machine. Specific temperatures and flow rates of a domestic washing machine have been used in the design procedure. Influence of different parameters were analysed in Fig. 7: i) the PCM plate storage unit configuration, based on a single-pass (sp) and a multi-pass (mp) arrangement; ii) the relative flow direction between charge and discharge, counter-current (cc) and co-current (co); iii) use of different kind of PCMs (an inorganic PCM1 and an organic PCM2 were used, both with similar melting temperature); iv) number of PCM plate capsules used; and v) the duration of the thermal charge process. The dimensionless heat recovered, which is evaluated as $\Omega = Q_{recovery}/Q_{reference}$, was used to identify the thermal performance of the different alternatives simulated, using as reference the heat obtained with a configuration based on 10 plates of PCM2, a multi-pass arrangement and a counter-current flow.

The first and second group of bars in Fig. 7 correspond to the performance study in function of the PCM plate numbers and flow arrangement (or configuration), fixing the PCM1 and co-current flow. The third and fourth group of bars show the thermal performance in function of the PCM plate numbers and the relative flow direction, fixing the PCM2 and multi-pass configuration. The fifth and sixth group of bars correspond to the performance results in function

of charge process time (time 1 = 50 seconds and time 2 = 170 seconds), using 10 PCM plates, multi-pass configuration and counter-current flow.

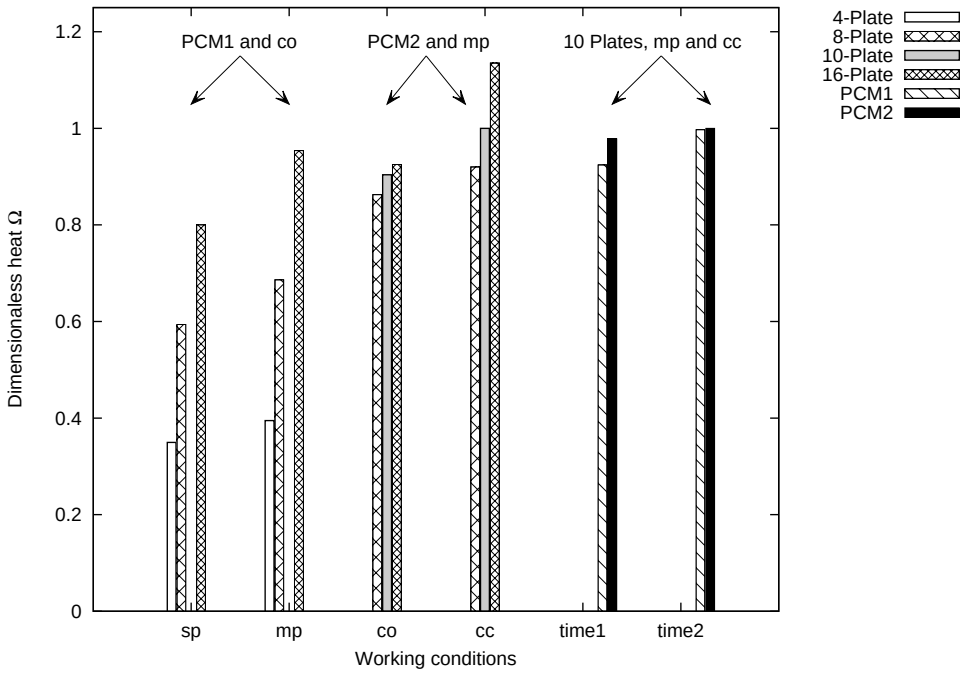


Fig. 7. Pre-design results of the storage unit performance

Analysing the numerical results the highest heat recovery is obtained with a multi-pass configuration, applying counter-current flow and using 16 PCM plate capsules. The relation between heat recovery and the number of PCM plates is directly proportional, but it is not lineal. Looking at the previous results, for PCM2, mp and co-current flow, the benefit of adding 2 PCM plates (from 8 to 10) and 6 PCM plates (from 10 to 16) only produces a heat recovery increase of 4.5% and 2.1%, respectively. Focusing on counter-current flow configuration, which produces a heat recovery increase compared to co-current flow configuration, the profit of adding 2 PCM plates (from 8 to 10) and 6 PCM plates (from 10 to 16) produces a heat recovery increase of 8.0% and 13.0%, respectively. This increase has been considered in the evaluation of an efficient design taking into account the technical limitations of space and weight, and the price of the PCM. After that, 10 PCM place capsules of PCM2 using a counter-current flow and multi-pass configuration were chosen

to configure the PCM plate heat storage unit.

## 6 Results

A group of tests has been carried out by means of the experimental facility with the aim of evaluating the thermal performance of the PCM plate heat storage unit. The numerical results have then been compared with the experimental data, evaluating the numerical discrepancy of the model proposed.

Dimensionless temperature, length and thickness are used in results description, being defined as: $\Phi = (T - T_{min})/(T_{max} - T_{min})$, $z^* = z/L$ and $y^* = y/L$, where $T_{min}$ is the low temperature, $T_{max}$ is the high temperature value and $L$ is the developed length of the PCM plate heat storage unit.

### *6.1 Test conditions*

The experiments and the numerical simulation of the PCM plate heat storage unit were carried out for three different mass flow rates and two different temperatures at the inlet of the unit, which value depends on the thermal process (charge or discharge). There is a difference of 20°C at the inlet temperature during the thermal charge and discharge process, and the fluid volume used during thermal charge was 70% of the fluid volume used in thermal discharge. Both conditions are imposed by the household application studied (a washing machine). The operating/working conditions used during thermal charge and discharge in function of the technical requirements are summarized in Table 3.

Table 3

Test definition: working conditions

| Process | Case | Time $[s]$ | Mass flow rate $[kg/s]$ | $\Phi$ |
|---|---|---|---|---|
| Thermal charge | A | 90 | 0.1554 | 1.0 |
| | B | 120 | 0.1166 | 1.0 |
| | C | 170 | 0.0823 | 1.0 |
| Thermal discharge | A/B/C | 170 | 0.1176 | 0.0 |

### *6.2 Global thermal analysis of the PCM plate heat storage unit*

The heat transfer between water flow and PCM plate heat storage unit is evaluated in function of the mass flow and difference between inlet and outlet fluid temperature during the transient process. The experimental thermal energy quantified for the three different cases during thermal charge and discharge are detailed in Table 4, as well as the numerical results and their discrepancy with respect to experimental data.

The PCM plate heat storage unit designed is capable of storing approximately 75% of the thermal energy contained in the drain water, which was produced in the first stage of a washing machine, and recovering part of it to supply around 50% of the thermal energy required to heat up a mass of water used in a next stage of the washing machine. These percentages are evaluated taking into account the relations between the thermal energy stored and a wasted heat obtained from the drain water (880 $kJ$), and between the thermal energy stored and the maximum heat storage capacity of the unit (1168 $kJ$) for the thermal charge process. The percentage of thermal energy recovered in relation to the maximum recovery heat (1672 $kJ$), and to the maximum heat storage capacity of the unit (1548 $kJ$) are also considered for the thermal discharge process. The maximum heat storage capacities of the unit during

thermal charge and discharge are different as a consequence of thermal conditions imposed by the domestic washing machine analysed (dimensionless temperature range and flow rate).

Table 4

Experimental data and numerical results of three cases studied

| Thermal charge (case) | Exp. heat transfer $[J]$ | Percentage vs. wasted heat [٪] | Percentage vs max. heat storage capacity [٪] | Num. heat transfer $[J]$ | Discrepancy [٪] | Average melting fraction |
|---|---|---|---|---|---|---|
| A | 682086 | 77.70 | 58.36 | 655236 | -3.93 | 0.65 |
| B | 649838 | 74.03 | 55.60 | 666395 | 2.55 | 0.70 |
| C | 662136 | 75.43 | 56.65 | 709833 | 7.20 | 0.80 |
| **Thermal discharge (case)** | **Exp. heat transfer $[J]$** | **Percentage vs. max. recovery [٪]** | **Percentage vs max. heat storage capacity [٪]** | **Num. heat transfer $[J]$** | **Discrepancy [٪]** | **Average melting fraction** |
| A | 799816 | 47.81 | 51.65 | 746106 | -6.71 | 0.18 |
| B | 791319 | 47.30 | 51.10 | 752910 | -4.85 | 0.21 |
| C | 801731 | 47.92 | 51.77 | 774860 | -3.35 | 0.25 |

The maximum heat storage capacity is evaluated adding the heat storage capacity of the PCM plates and the water mass contained into the heat storage unit. A PCM mass of 4.81 $kg$ with a heat storage capacity of 174 $kJ/kg$ (combination of latent and sensible heat in a dimensionless temperature range from 0.0 to 1.0), and a water mass of 8.5 $kg$ were used.

It is important to note that the thermal energy recovered during thermal discharge does not have to be the same as thermal energy stored because the unit

worked at different conditions (fluid volume, and dimensionless temperature range) during thermal charge and discharge.

Using the numerical model proposed in this paper, the thermal energy stored and recovered in the three cases have been evaluated. These values have been compared with experimental data, obtaining a maximum difference of 7,2% for case C during thermal charge, and 6,71% for case A during thermal discharge. The difference has been evaluated by means of the following formula: $Discrepancy(\%) = [(X_{Exp} - X_{Num})/X_{Exp}] * 100$.

In general an over-prediction of the thermal performance of the PCM plate heat storage unit during thermal charge is described, whilst a numerical under-prediction is found when thermal discharge process is simulated.

Although the global values obtained numerically show reasonable discrepancies, the short global variations between cases A, B and C are not coherent between experimental data and numerical results. Whilst the numerical results show an increase of the energy stored in function of the period of time during thermal charge (Cases A, B and C), the experimental data do not describe the same tendency. This experimental difference between cases could be seen as a consequence of the experimental procedure carried out and initial conditions used, together with the influence of the experimental uncertainty produced in the measuring of variables. The experimental uncertainty was evaluated obtaining a value around of $\pm 5\%$ for the energy stored/recovered, which can justify the variability in the experimental results.

Energy difference between cases A, B and C during thermal discharge is less than energy difference during thermal charge. It is due to the mass flow rate is very similar for all cases during thermal discharge. However, the smaller difference of thermal energy recovered between all cases can be explained as a consequence of the inlet fluid temperature profiles and the initial map

conditions (temperature and melting fraction of the PCM), which are different between them. The average melting fraction evaluated numerically gives the proportion of PCM which was melted at the final time step of each one of the thermal processes.

The heat recovery ratio is defined as a relation between the heat recovery measured and the available or wasted heat. In order to compare the heat recovery ratio of the PCM plate heat storage unit with some DWHR systems referenced in technical literature, a new available or wasted heat has been defined. It is due to the different operating/working conditions used during thermal charge and discharge. The new available or wasted heat (1170 $kJ$) has been evaluated applying the same mass drain water used during thermal charge, but considering a difference dimensionless temperature from 1 to 0 (instead of real charge limits from 1 to 0.3). The heat recovery ratio obtained experimentally for the PCM plate heat storage unit gives 67% , its relation gives similar values to highest heat recovery ratios reported in technical literature by different researchers in the field of DWHR systems [23, 28–33]. They have reported heat recovery ratios between 15-50% for DWHR devices based on double pipes, 35-75% for DWHR devices based on falling film and 38-55% for a DWHR device based on a cylindrical tank (depending on the kind of device, the orientation and the magnitude of the wasted water flow rate).

This analysis shows that the PCM plate heat storage unit designed accumulated thermal energy giving a competitive heat recovery ratio value in comparison with values reported in the field of DWHR systems. The PCM plate heat storage unit is capable to accumulate heat and releasing it later (not simultaneously), achieving a storage device in contrast with other DWHR systems which are configured to work only as demand devices (DWHR based on pipe heat exchanger). It is an important aspect that should be taken into account in the applicability of the unit designed, not only as a heat recovery system, but

also as a storage unit, which can be used to save energy during water heating process in different and real household applications, i.e.: washing machines or dishwashers.

### *6.3 Transient thermal analysis of the PCM plate heat storage unit*

The transient behaviour of the PCM plate heat storage unit has been analysed using the experimental testing and the numerical simulation. The transient boundary conditions imposed in the numerical code assume the same values obtained from experimental data, where dimensionless inlet fluid temperature were near to 0.3 and 1.0 during thermal charge and to 0.0 and 1.0 during thermal discharge.

The experimental and numerical inlet and outlet fluid temperature evolution, together with the heat transfer rate are depicted in Fig. 8 for the three cases (A, B and C) during *thermal charge*. The numerical outlet fluid temperature shows a constant value in a first period of time, which depends on the time required to remove the water volume stored previously into the test unit, whilst the experimental outlet fluid temperature describes a small increase during the first period of time, maybe due to an internal leakage/bypass effect, Fig. 8 (left). After that point, the numerical and experimental outlet fluid temperature begins to increase their value constantly until the final time describing the same tendency.

A high experimental heat transfer value obtained in case A regarding cases B and C (see Table 4) can be explained as a consequence of inlet fluid temperatures, in which the inlet fluid temperature profile of case A presents a higher value than cases B and C as a result of the experimental set-up, Fig. 8 (left). The numerical heat transfer does not reproduce the same effect, possible reasons were mentioned above (the influence of the numerical model hypothe-

sis and empirical correlation). Regarding the heat transfer difference between cases B and C, it can be explained from the time used in case C to exchange the thermal energy, which is higher than case B in spite of the heat transfer coefficient of case B is higher than case C.

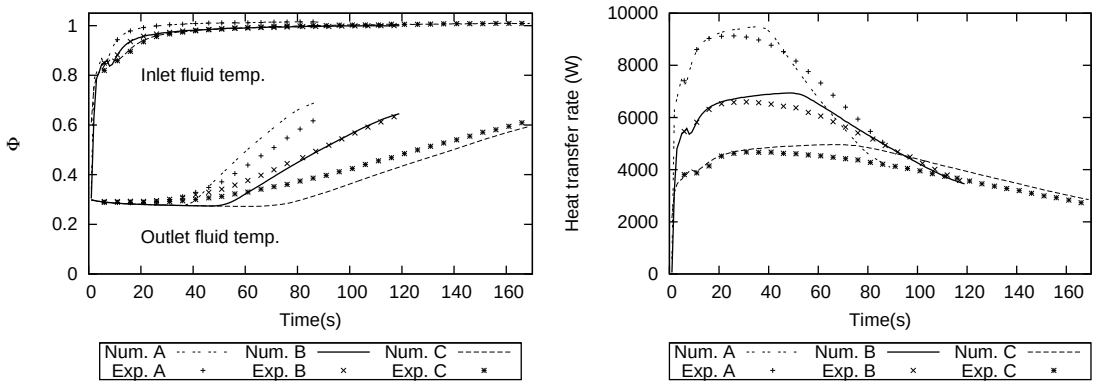


Fig. 8. Experimental data and numerical results during thermal charge: the fluid temperatures at the inlet and outlet (left); and heat transfer rate (right)

Difference between numerical result and experimental data of the outlet fluid temperature evolution can be seen along time Fig. 8(left). This difference produced an under-prediction in the numerical evaluation of the heat transfer rate in the case A and an over-prediction in the cases B and C (Table 4). Although the outlet fluid temperature and heat transfer difference, the thermal behaviour in transient conditions of the unit is well characterised by the numerical model, which describes the same tendency of the experimental data.

It is important to note that the results of the thermal charge process at final time step are used as initial conditions of the thermal discharge process. Therefore, the experimental and numerical results of the thermal discharge depend on the thermal behaviour of the thermal charge.

The experimental and numerical inlet and outlet fluid temperature evolution, together with the heat flux are depicted in Fig. 9 for the three cases (A, B and C) during *thermal discharge*. The numerical outlet fluid temperature evolution during thermal discharge present a constant and lineal decrease during the

first 50 seconds, which could be seen as the time required by the water volume stored previously to get out of the test unit. After that point, the decrease suffers a change in the gradient up to 70 seconds. This period of time is required to cool the PCM from initial temperature condition to the PCM solidification temperature, in which only sensible heat is working in the PCM. A progressive decrease is then maintained until final time. This period of time (70 to 170 seconds) can be understood as the time in which the fluid flow exchanges heat with the PCM plate storage unit taking advantage of the sensible and the latent heat.

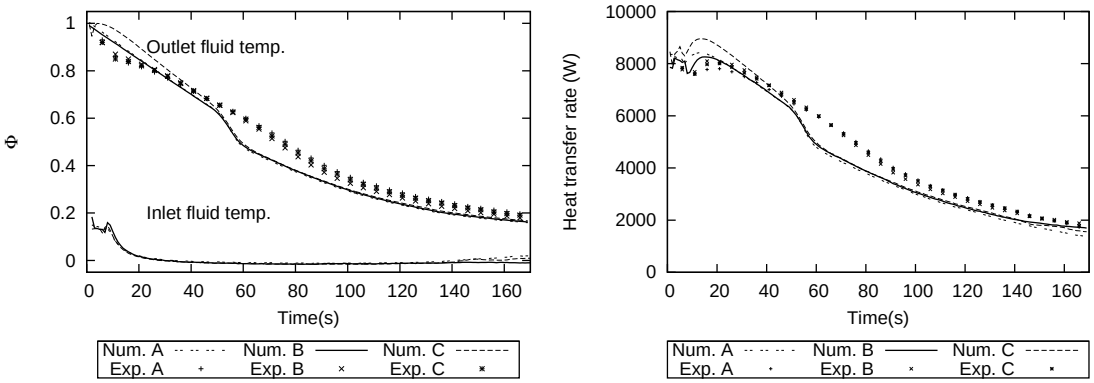


Fig. 9. Experimental data and numerical results during thermal discharge: the fluid temperatures at the inlet and outlet (left); and heat transfer rate (right)

A lower thermal energy recovered in case A is evaluated numerically in comparison with cases B and C, whilst a lower thermal energy recovered experimentally is obtained in case B (Table 4). A small difference between experimental heat transfer rate evaluated for the three cases tested can be explained from small difference of the inlet fluid temperature during the first 20 seconds, and later from 140 seconds until the final time (see Fig. 9 (left)), without forgetting the thermal condition of the PCM plates after carrying out the thermal charge process, which influence the instantaneous evaluation of the heat transfer rate.

The difference between the numerical results and experimental data during thermal charge and discharge could be explained as follows: i) the numerical model used to evaluate the fluid flow assumes an one-dimensional fluid flow

hypothesis, which does not allow to simulate the effect of mixture flow or irregular motion of the fluid in each one of the channels, and the influence of these phenomena on the evaluation of the fluid temperature along time; ii) the mass flow and the influence on the empirical evaluation of the heat transfer coefficient, which is used to evaluate the convective heat flux between fluid flow and PCM-plate and has been adopted from an intermating plate (approximation to the PCM plate used in the unit); iii) a possible water drain between PCM plate and metallic box or shell; and iv) the validity of adiabatic conditions at the edges of the PCM plate, and between fluid flow and shell considered in the numerical model.

In spite of this difference, similar temperature profiles are obtained numerically and experimentally for all three cases, and a good agreement is achieved at the final time.

### *6.4 Numerical results about PCM*

As an illustrative result of the level of information given by the numerical analysis of the encapsulated PCM, details of its behaviour are presented for case C.

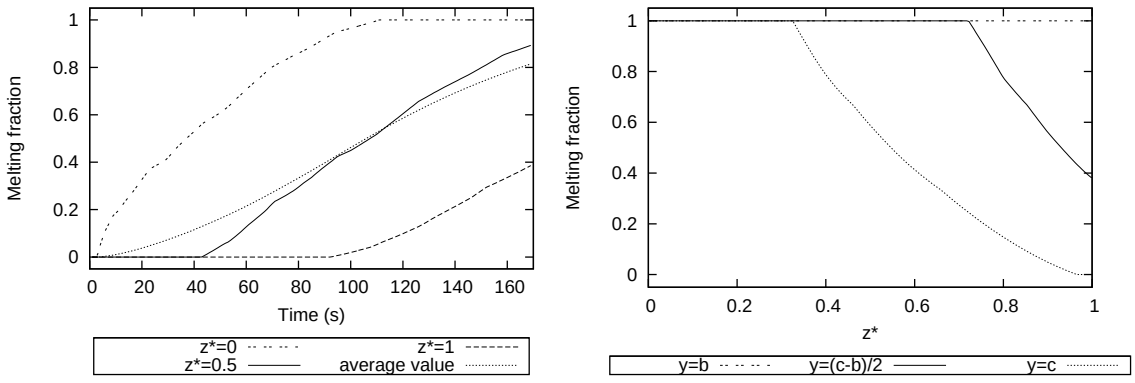


Fig. 10. PCM melting fraction: evolution during thermal charge and final distribution at time step 170 seconds (Case C)

The numerical results of the PCM melting fraction during thermal charge are shown in Fig. 10. The PCM melting fraction evolution is evaluated on three different longitudinal positions (z*=0, z*=0.5 and z*=1), together with the PCM melting fraction distribution in function of the PCM thickness (y=b, y=(c-b)/2 and y=c) at final instant.

The PCM melting fraction increases from 0 to 1 easily in zones near to the inlet of the fluid flow ($z^*$=0), whilst this behaviour is slower in zones near to the outlet of the fluid flow ($z^*$=1). It is a consequence of the fluid volume contained previously in the heat storage unit, together with the lower $\Delta$T at this point.

The PCM melting fraction value close to the outlet of the fluid flow ($z^*$=1) is zero during a period of time, after that a progressive increase occurs from 0 to a value close to 0.4. This gradient change is related to the total draining of the fluid volume stored previously into the PCM heat storage unit, which takes different times to flow out of the unit in function of the case (see Fig. 8 (left)). There is a short delay between times required to drain the water volume of the unit and the gradient change, it can be explained as the time required to increase the PCM temperature from initial condition of the fluid volume stored to the melting temperature. The same behaviour for the melting fraction at the middle length ($z^*$=0.5) is observed.

A PCM melting fraction average value has been evaluated numerically to characterize a general PCM thermal behaviour during thermal charge in function of time. As seen in Table 4, using a long period of time to carry out the thermal charge gives a better thermal behaviour of the PCM (higher average melting fraction). This observation is supported with the numerical results of the PCM melting fraction in function of thickness at final time step (see Fig. 10 right). The PCM melting fraction value at first PCM layer (y=b) is 1.0 along the total length, which means that the first layer of PCM is melted at the end of

the thermal charge, whilst this value at the middle thickness (y=(c-b)/2) and the biggest thickness (y=c) indicate that not all the PCM is being melted at the end of the test.

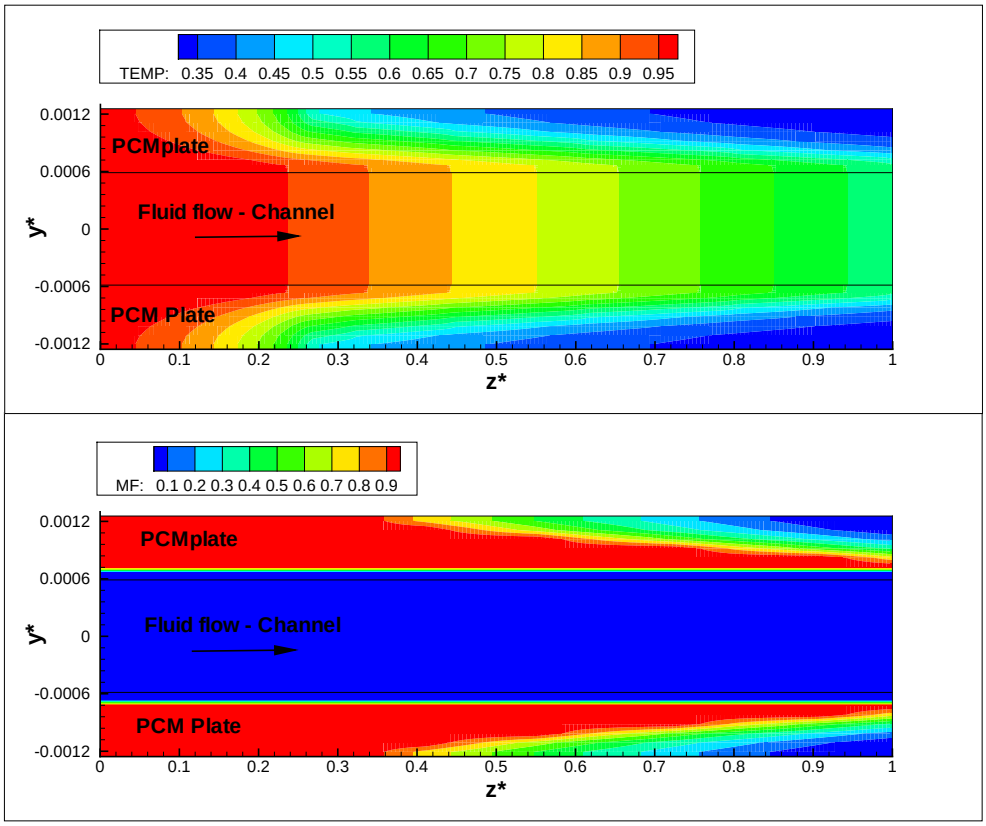


Fig. 11. Temperature distribution of the PCM plate and fluid flow, and PCM melting fraction at the final time step (170 seconds) of the thermal charge (Case C)

Fig. 11 gives detailed temperature and melting fraction maps for the final instant of the charge process, where the effect of low PCM thermal conductivity can be identified.

Regarding thermal discharge, Fig. 12 shows the numerical results of the PCM melting fraction evolution on three different longitudinal positions, together with the PCM melting fraction distribution in function of the thickness at final instant.

The PCM melting fraction value decreases along the period of time analysed

as a consequence of the heat flux transferred between fluid flow and PCM plate. The PCM melting fraction value at the inlet ($z^*$=1) falls from 0.4 to 0.0, maintaining this last value until final time. The melting fraction tendency at the outlet ($z^*$=0) is maintaining constant until 80 seconds, after that it falls from 1.0 to 0.6.

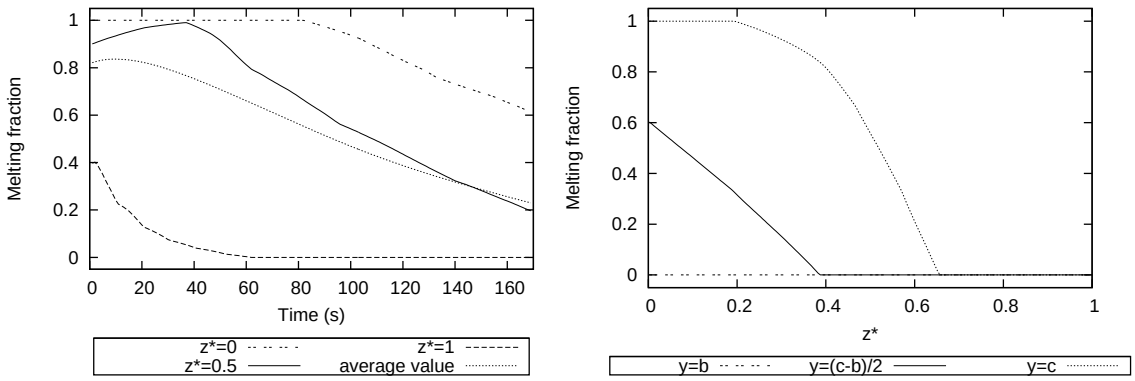


Fig. 12. PCM melting fraction: evolution during thermal discharge and final distribution at time step 170 seconds (Case C)

The PCM melting fraction in the middle of dimensionless length ($z^*$=0.5) increases its value during 40 seconds, after that a gradient change occurs and the value decreases until the final time step. The initial increase of the melting fraction is a consequence of the fluid volume contained previously into PCM plate heat storage unit (which is at final thermal conditions of the thermal charge simulation), and the flowing in counter-current direction. Once the fluid flow does not transfer more thermal energy to the PCM plate, the PCM begins to transfer the thermal energy stored to the fluid and PCM melting fraction begins to decrease.

The PCM melting fraction distribution in function of the thickness at final time step (Fig. 12 (right)) describes how the PCM is in solid state at first PCM layer, whilst other PCM layers show that they are still in the phase change process. This means that a part of the thermal energy stored during thermal charge is still in the PCM at the end of the thermal discharge process. The thermal discharge is conditioned by the initial thermal conditions, which

are obtained from thermal charge process. Thus, more time used during the thermal charge process gives as a result more thermal energy recovered during thermal discharge. The PCM average melting fraction is slightly higher (0.25 for case C and 0.18 for case A) (Table 4), but the change from charge to discharge is higher for case C (from 0.8 to 0.25) than for case A (from 0.65 to 0.18).

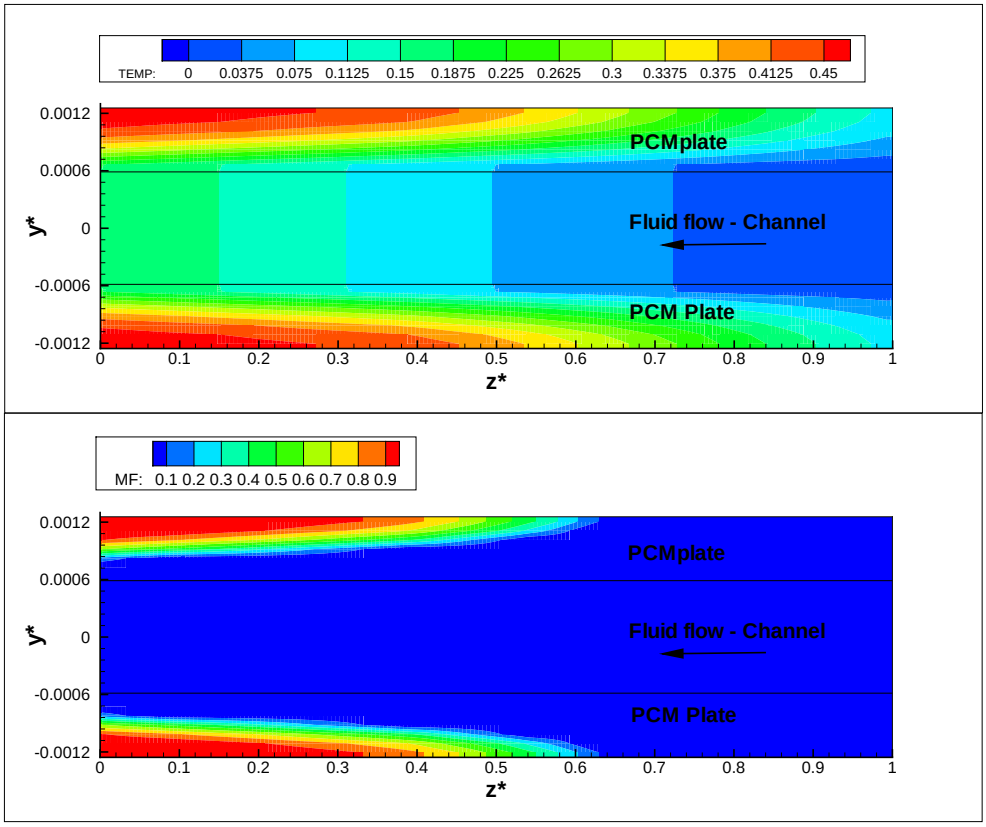


Fig. 13. Temperature distribution of the PCM plate and fluid flow, and PCM melting fraction at the final time step (170 seconds) of the thermal discharge (Case C)

Fig. 13 gives detailed temperature and melting fraction maps for the final instant of the discharge process, where the effect of low PCM thermal conductivity can be identified.

## 7 Conclusions

A drain water heat recovery/storage unit based on PCM plates was studied and designed using two different tools: numerical simulation and experimental testing. After analysing the global and transient thermal behaviour of the heat storage unit, a maximum heat of 800 $kJ$ has been recovered from a drain water heat source produced in the first stage of a washing machine. The PCM heat storage unit designed is capable to recover part of the stored energy to supply around 50% of the thermal energy required to heat up in a next stage of a washing machine (a real household application studied).

The relation between the thermal energy stored (measured) and the wasted heat was used to evaluate the heat storage ratio, which is around 75% . A similar relation between the thermal energy recovered (measured) and the wasted heat (adapted to the difference dimensionless temperature from 1 to 0) was used to evaluate the heat recovery ratio, which is around 67% . The heat recovery ratio of the unit designed gives similar value to highest heat recovery ratio reported in the field of DWHR systems.

The comparative analysis between numerical results and experimental data for three cases presents a reasonable good agreement, obtaining a maximum discrepancy of 7.2% during both thermal charge and discharge steps.

The numerical average melting fraction of the PCM heat storage unit reports that a part of the PCM was still melted at the final time of thermal discharge. It means that, if available, slimmer PCM plate capsules should be used with the aim of taking advantage of all PCM during transient processes (if the time used in each process, thermal charge and discharge, should be maintained as a technical specification of the problem studied).

The thermal performance study gives that the quantity of thermal energy re-

covered for the drain water heat recovery/storage unit designed is quite similar for all three cases. However, the numerical results predict a light dependence of the time spent for the thermal charge on the heat recovered. Although the experimental data does not give complete support to this idea, the thermal energy recovered during thermal discharge for cases A and B was lower than case C. This can be understood as less time spent for the thermal charge means wasting the PCM latent heat, which decreases the quality of the thermal storage.

The DWHR based on PCM plates designed and coupled to a washing machine represents a good alternative to save energy at household level. Also, the parallelepiped-shaped outer casing configuration gives facility to couple this storage unit into a washing machine or dishwasher body.

*Acknowledgement*

The authors gratefully acknowledge the financial support provided by Ministerio de Economía y Competitividad, Secretaría de Estado de Investigación, Desarrollo e Innovación, Spain (references. n$^o$. ENE2010-17801 and CEN-20091005) and the Torres Quevedo Programme.

## NOMENCLATURE

| | |
|---|---|
| A | cross section area ($m^2$) |
| CV | control volume |
| $e$ | specific total energy ($J\ kg^{-1}$) |
| g | acceleration of gravity ($m\ s^{-2}$) |
| h | specific enthalpy ($J\ kg^{-1}$) |
| H | plate width ($m$) |
| l | plate length ($m$) |
| L | developed length ($m$) |
| $\alpha$ | heat transfer coefficient ($Wm^{-2}K^{-1}$) |
| $\dot{m}$ | mass flow rate ($kg\ s^{-1}$) |
| m | mass ($kg$) |
| p | pressure ($Pa$) |
| $\dot{q}$ | heat flux ($W\ m^{-2}$) |
| T | temperature ($^oC$) |
| V | volume ($m^3$) |
| v | velocity ($m\ s^{-1}$) |
| $\Delta t$ | time step ($s$) |
| $\Delta z$ | control volume length (m) |

| | |
|---|---|
| $\lambda$ | thermal conductivity ($W\ m^{-1}K^{-1}$) |
| $\rho$ | density ($kgm^{-3}$) |
| $\tau_w$ | shear stress ($N\ m^{-2}$) |
| $\theta$ | inclination ($rad$) |
| Superscripts | |
| s | evaluated on staggered CV |
| Subscripts | |
| e,w,n,s | east, west, north and south CV-faces |
| P | main grid node associated to main CVs |
| E,W,N,S | nearest east, west, north and south nodes associated to main grid node P |

## References


[1] X.Q. Zhai, X.L. Wang, T. Wang, R.Z. Wang, A review on phase change cold storage in air-conditioning system: Materials and applications, Renewable and Sustainable Energy Reviews, Vol. 22, pp. 108-120, 2013.

[2] F. Agyenim, N. Hewitt, Eames P. and M. Smyth, A review of materials, heat transfer and phase change problem formulation for latent heat thermal energy storage system (LHTESS), Renewable and Sustainable Energy Reviews, Vol. 14, pp. 615-628, 2010.

[3] K.A.R. Ismail, and R. Stuginsky, A parametric study on possible fixed bed models for PCM and sensible heat storage, Applied Thermal Engineering, Vol. 19, pp. 757-788, 1999.

[4] K.A.R. Ismail, and A. Batista de Jesus, Parametric study of solidification of PCM around a cylinder for ice-bank applications, International Journal of Refrigeration, Vol. 24, pp. 809-822, 2001.

[5] M.M. Farid, A.M. Khudhair, S. Razack, and S. Al-Hallaj, A review on phase change energy storage: material and applications, Energy Conversion and Management, Vol. 45, pp 1597-1615, 2004.

[6] R. Baetens, B.P. Jell and A. Gustavsen, Phase change materials for building applications: a state-of-the-art review, Energy and Buildings, Vol. 42, pp. 1361-1368, 2010.

[7] D. Zhou, C.Y. Zhao, and Y. Tian, Review on thermal energy storage with phase change materials (PCMs) in building applications, Applied Energy, Vol. 92, pp. 593-605, 2012.

[8] E. Oró, A de Gracia, A. Castell, M.M. Farid and L.F. Cabeza, Review on phase change materials (PCMs) for cold thermal energy storage applications, Applied Energy, Vol. 99, pp 513-533, 2012.

[9] A. F. Regin, S.C. Solanki and J.S. Saini, Heat transfer characteristics of

thermal energy storage system using PCM capsules: A review, Renewable and Sustainable Energy Reviews, Vol. 12, pp. 2438-2458, 2008.

[10] A. F. Regin, S.C. Solanki and J.S. Saini, An analysis of a packed bed latent heat thermal energy storage system using PCM capsules: Numerical investigation, Renewable Energy, Vol. 34, pp. 1765-1773, 2009.

[11] A. Sharma, V.V. Tyagi, C.R. Chen and D. Buddhi, Review on thermal energy storage with phase change materials and applications, Renewable and Sustainable Energy Reviews, Vol. 13, pp. 318-345, 2009.

[12] J. Wei, Y. Kawaguchi, S. Hirano and H. Takeuchi, Study on a PCM heat storage system for rapid heat supply, Applied Thermal Engineering, Vol. 25, pp. 2903-2920, 2005.

[13] P. Lamberg, R. Lehtiniemi, A. Henell, Numerical and experimental investigation of melting and freezing processes in phase change material storage, Int. Journal of Thermal Sciences, Vol. 43, pp. 277-287, 2004.

[14] S. Seddegh, X. Wang, A.D. Henderson, Z. Xing, Solar domestic hot water systems using latent heat energy storage medium: A review, Renewable and Sustainable Energy Reviews, Vol. 49, pp. 517-533, 2015.

[15] P. Dolado, A. Lazaro, J.M. Marin, and B. Zalba, Characterization of melting and solidification in real scale PCM-air heat exchanger: Numerical model and experimental validation, Energy Conversion and Management, Vol. 52, pp. 1890-1907, 2011.

[16] M. Nabavitabatabayi, F. Haghighat, A. Moreau, and P. Sra, Numerical analysis of a thermally enhanced domestic hot water tank, Applied Energy, Vol. 129, pp. 253-260, 2014.

[17] Y.B. Tao and Y.L. He, Numerical study on thermal energy storage performance of phase change material under non-steady-state inlet boundary, Applied Energy, Vol. 88, pp. 4172-4179, 2011.

[18] Y.Q. Li, Y.L. He, H.J. Song, C. Xu, W.W. Wang, Numerical analysis and parameters optimization of shell-and-tube heat storage unit using three phase change materials, Renewable Energy, Vol. 59, pp. 92-99, 2013.

[19] D. Haillot, E. Franquet, S. Gibout, and J.P. Bédécarrats, Optimization of solar DHW system including PCM media, Applied Energy, Vol. 109, pp. 470-475, 2013.

[20] P. Wang, X. Wang, Y. Huang, C. Li, Z. Peng and Y. Ding, Thermal energy charging behaviour of a heat exchanger device with a zigzag plate configuration containing multi-phase-change-material, Applied Energy, Vol. 142, pp. 328-336, 2015.

[21] K. Merlin, D. Delaunay, J. Soto, L. Traonvouez, Heat transfer enhancement in latent heat thermal storage systems: Comparative study of different solutions and thermal contact investigation between the exchanger and the PCM, Applied Energy, Vol. 166, pp. 107-116, 2016.

[22] M. Medrano, M.O. Yilmaz, M. Nogués, I. Martorrel, J. Roca, and L.F. Cabeza, Experimental evaluation of commercial heat exchangers for use as PCM thermal storage systems, Applied Energy, Vol. 86, pp. 2047-2055, 2009.

[23] A. McNabola, and K. Shields, Efficient drain water heat recovery in horizontal domestic shower drains, Energy and Buildings, Vol. 59, pp. 44-49, 2013.

[24] L. Liu, L. Fu, and Y. Jiang, Application of an exhaust heat recovery system for domestic hot water, Energy, Vol. 35, pp. 1476-1481, 2010.

[25] L. Liu, L. Fu, and S. Zhang, The design and analysis of two exhaust heat recovery systems for public shower facilities, Applied Energy, Vol. 132, pp. 267-275, 2014.

[26] J. Dong, Z. Zhang, Y. Yao, Y.Jiqiang, and B. Lei, Experimental performance evaluation of a novel heat pump water heater assisted with shower drain water, Applied Energy, Vol. 154, pp. 842-850, 2015.

[27] W. Wu, T. You, B. Wang, W. Shi, and X. Li, Simulation of a combined heating, cooling and domestic hot water system based on ground source absorption heat pump, Applied Energy, Vol. 126, pp. 113-122, 2014.

[28] S. Torras, C. Oliet, J. Rigola, and A. Oliva, Drain water heat recovery storage-type unit for residential housing, Applied Thermal Engineering, Vol. 103, pp. 670-683, 2016.

[29] J. Wallin, and J. Claesson, Investigating the efficiency of a vertical inline drain water heat recovery heat exchanger in a system boosted with a heat pump, Energy and Buildings, Vol. 80, pp. 7-16, 2014.

[30] I. Beentjes, R. Manouchehri, and M.R. Collins, An investigation of drain-side wetting on the performance of falling film drain water heat recovery systems, Energy and Buildings, Vol. 82, pp. 660-667, 2014.

[31] D. Slýs, and S. Kordana, Financial analysis of the implementation of a Drain Water Heat Recovery unit in residential housing, Energy and Buildings, Vol. 71, pp. 1-11, 2014.

[32] L. Ni, S.K. Lau, H. Li, T. Zhang, J.S. Stansburry, J. Shi, and J. Neal, Feasibility study of a localized grey water energy-recovery system, Applied Thermal Engineering, Vol. 39, pp. 53-62, 2012.

[33] L.T. Wong, K.W. Mui, and Y. Guan, Shower water heat recovery in high-rise residential buildings of Hong Kong, Applied Energy, Vol. 87, pp. 703-709, 2010.

[34] O. García, C.D. Pérez, J. Rigola, Numerical simulation of double pipe condensers and evaporators, International Journal of Refrigeration, Vol. 27 (6), pp. 656-670, 2004.

[35] S. Morales-Ruiz, J. Rigola, C.D. Pérez-Segarra and O. García-Valladares, Numerical analysis of two-phase flow in condensers and evaporators with special emphasis on single-phase/two-phase transition zones, Applied Thermal Engineering, Vol 29, pp. 1032-1042, 2009.

[36] S. Morales-Ruiz, J. Rigola, I. Rodriguez, A. Oliva, Numerical resolution of the liquid-vapour two-phase flow by means of the two-fluid model and a pressure based method, International Journal of Multiphase Flow, Vol 43, pp. 118-130, 2012.

[37] V. Voller and C. Prakash, A fixed grid numerical modelling methodology for convection-diffusion meshy region phase-change problem, Int. Journal Heat and Mass Transfer, Vol. 30, pp. 1709-1719, 1987.

[38] M. Costa, A. Oliva, C.D. Pérez-Segarra and R. Alba, Numerical simulation of solid-liquid phase change phenomena, Computer Methods in Applied Mechanics and Engineering, Vol. 91 (1-3), pp. 1123-1134, 1991.

[39] M. Costa, A. Oliva, C.D. Pérez-Segarra, A Three-Dimensional Numerical Study of Melting Inside an Isothermal Horizontal Cylinder, Numerical Heat Transfer, Part A (Applications) Vol. 32 (5), pp. 531-553, 1997.

[40] Y. Belhamadia, A.S. Kane, and A. Fortin, An enhanced mathematical model for phase change problems with natural convection, Int. Journal of Numerical Analysis and Modeling, Serie B, Vol. 3, Num. 2, pp. 192-206, 2012.

[41] A. Durmus, H. Benli, I, Kurbas and H. Gül, Investigation of heat transfer and pressure drop in plate heat exchangers having different surface profiles, Int. Journal of Heat and Mass Transfer, Vol. 52, pp. 1451-1457, 2009.

[42] K.J. Bell and Others, Heat exchanged design handbook 3 - Thermal and hydraulic design of heat exchangers, Hemisphere publishing Corporation, London, 1983.

[43] S. Kakac, H. Liu and K. Kakag, Heat exchangers: selection, rating and thermal design, CRC Press, 2002.

[44] S.V. Patankar, Numerical heat transfer and fluid flow, McGraw-Hill, NY, 1980.

[45] R.J. Moffat, Describing the uncertainties in experimental results, Experimental Thermal and Fluids Science, Vol. 1, pp. 3-17, 1998.

[46] H.W. Coleman and W.G. Steele, Experimentation and uncertainty analysis for engineers, John Wiley and Sons, Inc. New York, 1998.